Poincaré Return Maps in Neural Dynamics: Three Examples

Marina L. Kolomiets and ANDREY L. SHILNIKOV

Abstract Understanding of the onset and generic mechanisms of transitions between distinct patterns of activity in realistic models of individual neurons and neural networks presents a fundamental challenge for the theory of applied dynamical systems. We use three examples of slow-fast neural systems to demonstrate a suite of new computational tools to study diverse neuronal systems.

Keywords Neurodynamics · Poincaré return maps · Neural model · Networks

1 Introduction

Most neurons demonstrate oscillations of the membrane potential either endogenously or due to external perturbations. Deterministic description of primary oscillatory activities, such as tonic spiking and bursting, of neuronal dynamics is based on models following the Hodgkin-Huxley formalism [1]. Mathematically, such conductance based models belong to a special class of dynamical systems with at least two distinct time scales, the so-called slow—fast systems [2–8]. Bursting is a manifestation of slow–fast dynamics possessing subcomponents operating at distinct time scales. Neural bursting is a modular activity composed of various limiting branches, corresponding to oscillatory and equilibrium regimes of the fast subsystem, and

M. L. Kolomiets
Department of Mathematics, Academy of Agricultural Sciences, Nizhniy,
Novgorod 603107, Russia

A. L. SHILNIKOV (✉)
Neuroscience Institute, Department of Mathematics and Statistics, Georgia State University,
Atlanta, Georgia 30303, USA
e-mail: ashilnikov@gsu.edu
URL: https://labs.ni.gsu.edu/ashilnikov/

connected by transients between them. Using the common mathematical we can better understand the basic onset of bursting oscillations in models of individual and coupled neurons. The study of mechanisms of bursting and its transformations requires nonlocal bifurcation analysis, which is based on the derivation and further examination of Poincaré return maps.

## 2 Hodgkin-Huxley Type Model of a Leech Heart Interneuron

Our first example is the "reduced" model of heart interneuron model [9–13] derived through the Hodgkin-Huxley gated variables formalism [1] that not every mathematician may be familiar with. Its equations do look too detailed and overwhelming:

$$C \frac{dV}{dt} = -I_{\text{Na}} - I_{\text{K2}} + I_{\text{L}} - I_{\text{app}} - I_{\text{syn}}, \tag{1}$$

$$I_L = \bar{g}_{\text{L}} \, (V - E_{\text{L}}), \qquad I_{\text{K2}} = \bar{g}_{\text{K2}} \, m_{\text{K2}}^2 (V - E_{\text{K}}),$$

$$I_{\text{Na}} = \bar{g}_{\text{Na}} \, m_{\text{Na}}^3 \, h_{\text{Na}} \, (V - E_{\text{Na}}), \quad m_{\text{Na}} = m_{\text{Na}}^\infty(V),$$

$$\tau_{\text{Na}} \frac{dh_{\text{Na}}}{dt} = h_{\text{Na}}^\infty(V) - h, \quad \tau_{\text{K2}} \frac{dm_{\text{K2}}}{dt} = m_{\text{K2}}^\infty(V) - m_{\text{K2}},$$

where $C = 0.5$ nF is the membrane capacitance; V is the membrane potential; $I_{\text{N}a}$ is the fast voltage gated sodium current with slow inactivation h_{Na} and fast activation m_{Na}; I_{K2} is the persistent potassium current with activation m_{K2}; I_{L} is leak current and I_{app} is a constant polarization or external applied current. The maximal conductances are $\bar{g}_{\text{K2}} = 30$nS, $\bar{g}_{\text{Na}} = 200$nS and $g_{\text{L}} = 8$nS, and the reversal potentials are $E_{\text{Na}} = 0.045$ V, $E_{\text{K}} = -0.070$V and $E_{\text{L}} = -0.046$V. The time constants of gating variables are $\tau_{\text{K2}} = 0.25$ sec and $\tau_{\text{Na}} = 0.0405$ s. The steady state values of gating variables, $h_{\text{Na}}^\infty(V), m_{\text{Na}}^\infty(V), m_{\text{K2}}^\infty(V)$, are given by the following sigmoidal functions:

$$h_{\text{Na}}^\infty(V) = [1 + \exp(500(0.0333 - V))]^{-1}$$
$$m_{\text{Na}}^\infty(V) = [1 + \exp(-150(0.0305 - V))]^{-1} \tag{2}$$
$$m_{\text{K2}}^\infty(V) = [1 + \exp(-83(0.018 - V + V_{\text{K2}}^{\text{shift}}))]^{-1}.$$

The quantity $V_{\text{K2}}^{\text{shift}}$ is a genuine bifurcation parameter for this model: it is the deviation from experimentally averaged voltage value $V_{1/2} = 0.018$ V corresponding to semi-activated potassium channel, i.e. $m_{\text{K2}}^\infty(0.018) = 1/2$. Variations of $V_{\text{K2}}^{\text{shift}}$ move the slow nullcline $\frac{dm_{\text{K2}}}{dt} = 0$ in the V-direction in the 3D phase, see Fig. 1. Due to the disparity of the time constants of the phase variables, the fast-slow system paradigm is applicable to system (1): its first two differential equations form a fast subsystem, while the last equation is the slow one. The dynamics of such a system are known [14] to be determined by, and centered around, attracting pieces of the slow motion
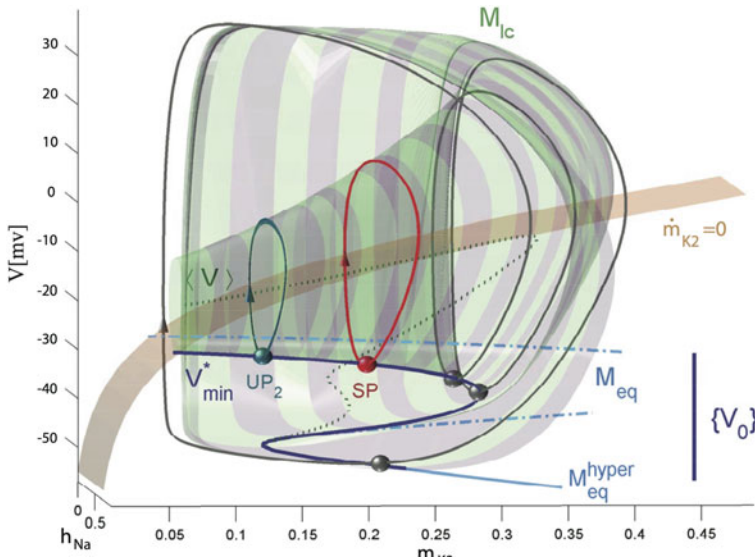
Fig. 1 Slow motion manifolds and nullclines of the model (1): the 2D spiking manifold M_{lc} is foliated by the periodic orbits continued, from the left to the right, as the parameter V_{K2}^{shift} is increased from -0.026 through 0.0018. The space curves V_{min} and $\langle V \rangle$ are made of minimal and average coordinates of the periodic orbits. M_{lc} glues to the hyperpolarized fold of the quiescent manifold, M_{eq}, comprised of the equilibrium states of (2), where the curve of the averaged values $\langle V \rangle$ terminates. An equilibrium state of Eqs. (2) is the intersection point of M_{eq} with the slow (yellow) nullcline $\dot{m}_{K2} = 0$ for given V_{K2}^{shift}. Also shown (in red) is the curve of the v-minimal coordinate values of the periodic orbits making M_{lc}. This curve is used to define the Poincaré map taking it onto itself after one revolution around M_{lc}

manifolds that constitute a skeleton of activity patterns. These manifolds are formed by the limit sets, such as equilibria and limit cycles, of the fast subsystem where the slow variable becomes a parameter in the singular limit.

A typical Hodgkin-Huxley model possesses a pair of such manifolds [15]: quiescent and tonic spiking, denoted by M_{eq} and M_{lc}, correspondingly. A solution of (2) that repeatedly switches between the low, hyperpolarized branch of M_{eq} and the spiking manifold M_{lc} represents a busting activity in the model. Whenever the spiking manifold M_{lc} is transient for the solutions of (1), like those winding around it in Figs. 2, the models exhibits regular or chaotic bursting. Otherwise, the model (1) has a spiking periodic orbit that has emerged on M_{lc} through the saddle-node bifurcation thereby terminating the bursting activity [16] or both regimes may co-exist as in [17, 18].

To determine what makes the spiking and bursting attractors change their shapes and stability, we construct numerically a V_{K2}^{shift}- parameter family of 1D Poincaré maps taking an interval of membrane potentials onto itself. This interval is comprised of the minimal values, denoted by $\langle V_0 \rangle$, of the membrane potential on the found periodic orbits foliating densely the spiking manifold M_{lc}, see Fig. 1. Then, for some V_{K2}^{shift}-
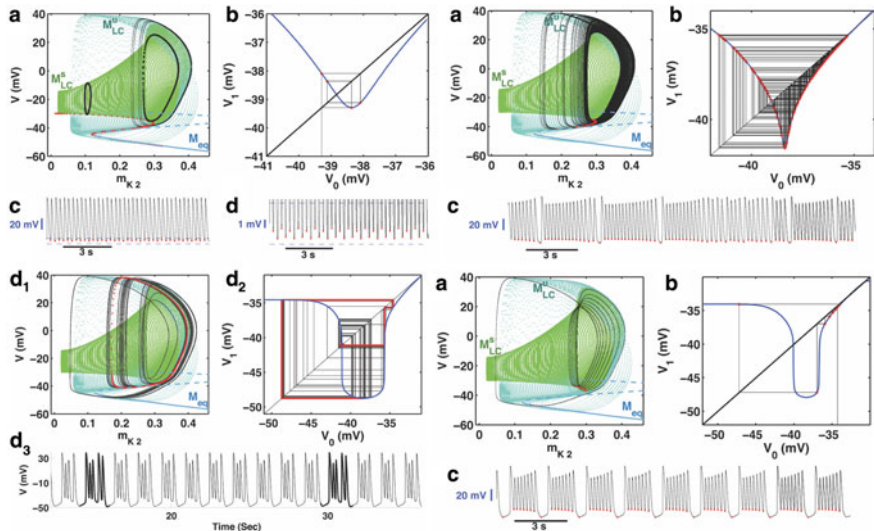
Fig. 2 (Top-left) Four v-minimums of the stable spiking periodic orbit spiking at $V_{K2}^{shift} = 0.0255$ corresponding to the period-4 orbit of the Poincaré map. Insets (C) and (D) show the voltage waveforms.(Top-right) Chaotic spiking of the model and in the map at $V_{K2}^{shift} = -0.0254$. (Bottom) Chaotic bursting at the spike adding transition becomes more regularized with a large number of spikes per burst

values, we integrate numerically the outgoing solutions of (2) starting from the initial conditions corresponding to each (V_0) to find the consecutive minimum (V_1) in the voltage time series. All found pairs (V_0, V_1) constitute the graph of the Poincaré map for given V_{K2}^{shift}.

Figure 2 is a showcase of such 1D unimodal maps with the distinctive U-shape. A fixed point of map would correspond to a single V-minimum on the periodic orbit on the 2D tonic spiking manifold, while period-2 orbit of the map corresponds to the periodic orbit of the model and so forth. A bursting orbit with multiple turns around M_{lc} and switching to and back from M_{lc} is represented by a more complex orbit of a longer period. Moreover, the bursting orbit may become even chaotic at spike adding transition, and as the map reveals that is caused by a homoclinic orbit (red trajectory) of an unstable fixed point corresponding to a saddle periodic orbit of the neural model (1). The shape of the 1D return map infers that as it becomes steeper with a characteristic cusp shape the model would move into the chaotic regime.

3   FitzHugh-Nagumo-Rinzel Model

Our next example is the FitzHugh-Nagumo-Rinzel (FNR) model which is a mathematical model of an elliptic burster (see Fig. 3B); its equations given by [19]:
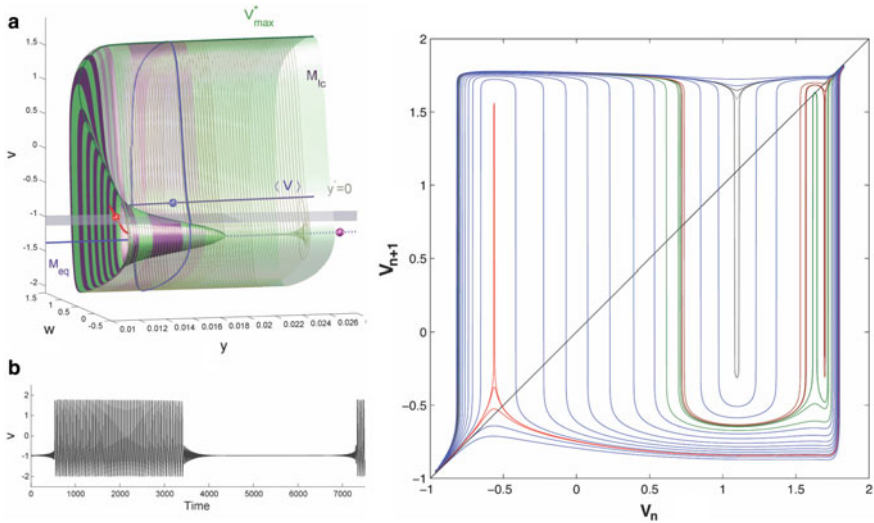
Fig. 3 (A) Topology of the tonic spiking, M_{lc}, and quiescent, M_{eq}, manifolds. The fold on M_{lc}, corresponds to a saddle-node bifurcation where the stable (outer) and saddle (inner) branches, comprised of periodic orbits, merge. The vertex, where the unstable branch of M_{lc} collapses at M_{eq}, corresponds to a subcritical Andronov-Hopf bifurcation. Space curves, labeled by V_{max}^* (in green) and $\langle V^{s,u} \rangle$ (in blue and red, respectively), correspond to the V-maximal and the averaged, over the period, coordinates of the periodic orbits composing M_{lc}. The plane, $y' = 0$, is the slow nullcline, above (below) which the y-component of a solution of the model increases (decreases). The plane is elevated/lowered as the c-parameter is increased/decreased. (right) The "continuously" reshaping family of the 1D Poincaré return maps $T : V_n \to V_{n+1}$ for the FHN-model at $\mu = 0.002$ as c increases from $c = -1$ through $c = -0.55$. Lower graphs correspond to quiescence and subthreshold oscillations in the model; upper graphs correspond to tonic spiking dynamics, while the middle graphs describe bifurcations of bursting. An intersection point of a graph with the bisectrix is a fixed point of the map. The stability of the fixed point is determined by the slope of the graph, i.e. it is stable if $|T'| < 1$

$$v' = v - v^3/3 - w + y + I,$$
$$w' = \delta(0.7 + v - 0.8w),$$
$$y' = \mu(c - y - v). \tag{3}$$

Here, $\delta = 0.08$, $I = 0.3125$ is an "external current", and we set $\mu = 0.002$ determining the pace of the slow variable y; the bifurcation parameter of the model is c.

The slow variable y becomes frozen when $\mu = 0$. The first two fast equations in (3) compose the FitzHugh-Nagumo fast subsystem model describing a relaxation oscillator, provided δ is small. This subsystem exhibits either tonic spiking on a stable limit cycle, or quiescence on a stable equilibrium state for some fixed values of y. Stability loss of the equilibrium state in the fast subsystem gives rise to a stable limit cycle through a sub-critical Andronov-Hopf bifurcation when an unstable limit cycle collapses into the equilibrium state. The stable and unstable limit cycle emerge in the FNR-model through a saddle-node bifurcation. Both bifurcations, Andronov-Hopf

and saddle-node, are key to the description of an elliptic burster. Using a traditional slow-fast dissection, one can locate the corresponding branches of the limit cycle and equilibrium states by varying the frozen y-variable in the extended phase space of the fast subsystem. The topology of the tonic spiking, M_{lc}, and quiescent, M_{eq}, in the phase space the FNR-model is revealed in Fig. 3.

4 1D Voltage Maps

Recall that a feature of a slow-fast system is that its solutions are constrained to stay near the slow-motion manifolds, composed of equilibria and periodic obits of the fast subsystem. If both manifolds are transient for the solutions of the corresponding neuron model, it exhibits a bursting behavior, which is a repetitive alternation of tonic spiking and quiescent periods. Otherwise, the model demonstrates the tonic spiking activity if there is a stable periodic orbit on the tonic spiking manifold, or it shows no oscillations when solutions are attracted to a stable equilibrium state on the quiescent manifold.

The core of the methods is a reduction to, and a derivation of, a low dimensional Poincaré return map, with an accompanying analysis of the limit solutions: fixed, periodic and homoclinic orbits, representing various oscillations in the original model. Maps have been actively employed in computational neuroscience, see [20–23] and referenced therein. It is customary that such a map is sampled from voltage traces, for example by singling out successive voltage maxima or minima, or interspike intervals. A drawback of a map generated by time series is a sparseness, as the construction algorithm reveals only a single periodic attractor of a model, unless the latter demonstrates chaotic or mixing dynamics producing a large variety of densely wandering points.

A new, computer assisted method for constructing a complete family of Poincaré maps for an interval of membrane potentials for slow-fast Hodgkin-Huxley models of neurons was proposed in [12] following [24], see above. Having such maps we are able to elaborate on bifurcations in the question of tonic spiking and bursting, detect bistability, as well examine unstable sets, which are the organizing centers of complex dynamics in any model. Using this approach we have studied complex bursting transformations in a leech heart interneuron model and revealed that the cause of complex behaviors at transitions is homoclinic tangles of saddle periodic orbits which can be drastically amplified by small noise [11, 25]. Examination of the maps will help us make qualitative predictions about transitions *before* they actually occur in the models.

The construction of the voltage interval maps is a two stage routine. First, we need to accurately single out the slow motion manifold M_{lc} in the neuronal model using the parameter continuation technique. The manifold is formed by the tonic-spiking periodic orbits as a control parameter in the *slow* equation is varied. Recall, that its variations, raising or lowering the slow nullcline in the phase space of the model, do not alter the fast subsystem and hence do keep the manifold intact. Next a space

curve V^*_{max} on M_{lc} is detected, which corresponds to maximal voltage values of the membrane potentials V_n found on all periodic orbits constituting the tonic spiking manifold, see Fig. 3.

We use this data to further amend the set $\{V_n\}$, by integrating the solutions of the model in the vicinity of each maxima to find the exact locations of the turning points, determined by the condition $V'_{max} = 0$. Next, the points defining $\{V_n\}$ are employed as the initial conditions to compute outgoing solutions of (3) that will stay on or close to M_{lc}. The integration is stopped when a successive maximal value $\{V_{n+1}\}$ of the voltage is reached in the voltage trace. Figure 4 demonstrates how the shape of the 1D maps changes in a complex predictable way as the c-parameter is varied. One can see from the end points, that the map has initially a stable fixed point at the top-right corner that corresponds to the stable tonic spiking orbit on the outer surface of the 2D manifold M_{lc} in Fig. 3(left). One can also foresee from the map at the bottom-right corner in Fig. 3(right) the neural model will undergo a cascade of period-doubling bifurcations of sub-threshold oscillations followed by complex mixed-mode oscillations involving sub-threshold ones and bursting. Our predictions are illustrated and confirmed by Fig. 4 that samples four characteristic 1D Poincaré return maps out of Fig. 3. In it the shape of the 1D Poincaré return maps reveals the underlying cause of chaotic mixed mode oscillations (MMOs) at the transition from tonic spiking to bursting in the in the FNR-model (3) that next become periodic MMOs, and further transition to chaotic and regular sub-threshold oscillations en a route to the quiescent phase in generic elliptic bursters.

5 Example 3: 2D Recurrent Maps in Multifunctional 3-Cell Networks

Many rhythmic motor behaviors such as respiration, chewing, locomotion on land and in water, and heartbeat (in leeches) are produced by networks of cells called central pattern generators (CPGs). A CPG is a neural microcircuit of cells whose synergetic, nonlinear interactions can autonomously generate an array of multicomponent/polyrhythmic bursting patterns of activity that determine motor behaviors in animals, including humans [26–32]. Modeling studies, phenomenologically mathematical and exhaustively computational, have proven useful to gain insights into operational principles of CPGs [33–40]. Although various models, reduced and feasible, of specific CPGs, have been developed, it remains unclear how the CPGs achieve the level of robustness and stability observed in nature [41–45]. Understanding the key universal mechanisms of the functional evolution of neural connectivity, bifurcation mechanisms underlying transitions between different neural activities, and accurate modeling of these processes presents opportunity and challenge for applied mathematics in particular and for all computational sciences in general.

Whereas a dedicated CPG generates a single pattern robustly, a multifunctional or polymorphic CPG can flexibly produce distinct rhythms, such as temporally dis-
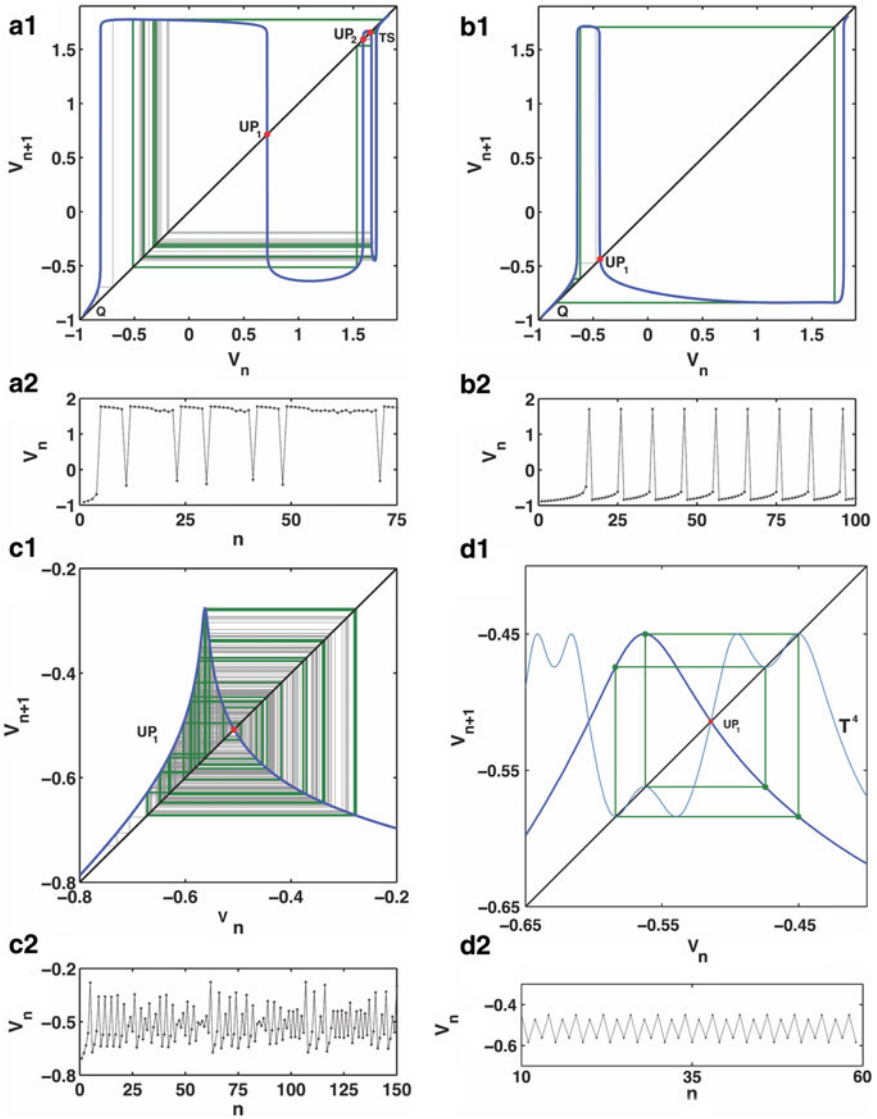
Fig. 4 (A1/2) The shape of the 1D Poincaré return map reveals the underlying cause of chaotic mixed mode oscillations (MMOs) at the transition from tonic spiking to bursting in the in the FNR-model (3) that become periodic MMOs with a single burst followed by nine sub-threshold oscillations (B1/2). (C1/2) The unimodal map corresponding to chaotic and period-4 sub-threshold oscillations (D1/2)

tinct swimming versus crawling locomotions, and alternation of directions of blood circulation in leeches [46–48]. Switching between various attractors of a CPG network causes switching between locomotion behaviors. Each attractor is associated with a definite rhythm running on a specific time scale with well-defined and robust phase lags among the constituting neurons. The emergence of synchronous rhythms in neural networks is closely related to temporal characteristics of coupled neurons due to intrinsic properties and types of synaptic coupling, which can be inhibitory, excitatory and electrical, fast and slow [49–53].

We developed a computational toolkit for oscillatory networks that reduces the problem of the occurrence of bursting and spiking rhythms generated by a CPG network to the bifurcation analysis of attractors in the corresponding Poincaré return maps for the phase lags between oscillatory neurons. The structure of the phase space of the map is an individual signature of the CPG as it discloses all characteristics of the functional space of the network. Recurrence of rhythms generated by the CPG (represented by a system of coupled Hodgkin-Huxley type neurons [54]) lets us employ Poincaré return maps defined for phase lags between spike/burst initiations in the constituent neurons (Fig. 5) [41, 49–51, 55]. Forward trajectories $\left\{ \phi_{21}^{(n)}, \phi_{31}^{(n)} \right\}$ of phase points $\mathbf{M}_n = \left(\phi_{21}^{(n)}, \phi_{31}^{(n)} \right)$ of the Poincaré map $\Pi : \mathbf{M}_n \to \mathbf{M}_{n+1}$ are defined through the time delays $\Delta\phi_{j1}^{(n)} = \dfrac{\tau_{j1}^{(n+1)} - \tau_{j1}^{(n)}}{\tau_1^{(n+1)} - \tau_1^{(n)}}$ (on mod 1) between the burst initiations in each cycle normalized over the network period, can converge to several co-existing stable fixed points, thus indicating the given network is multistable, or a single stable invariant circle wrapping around the torus that corresponds to a unique rhythmic outcome with periodically varying phase lags. These are attractors, single or multiple, of the return map on a 2D torus, which are associated with multifunctional or dedicated neural circuits, respectively (Fig. 5). The 2D return map, $\Pi : \mathbf{M}_n \to \mathbf{M}_{n+1}$, for the phase lags can be written as follows:

$$\phi_{21}^{(n+1)} = \phi_{21}^{(n)} + \mu_1 f_1 \left(\phi_{21}^{(n)}, \phi_{31}^{(n)} \right), \qquad \phi_{31}^{(n+1)} = \phi_{31}^{(n)} + \mu_2 f_2 \left(\phi_{21}^{(n)}, \phi_{31}^{(n)} \right) \qquad (4)$$

with μ_i representing the coupling strength, and f_i being some undetermined coupling functions such that $f_1 = f_2 = 0$ corresponds to its fixed points: $\phi_{j1}^* = \phi_{j1}^{(n+1)} = \phi_{j1}^{(n)}$. These functions, similar to phase-resetting curves, can be assessed from the simulated data collected for known all trajectories $\left\{ \phi_{21}^{(n)}, \phi_{31}^{(n)} \right\}$. By treating f_i as partials $\partial F / \partial \phi_{ij}$, we can restore a "phase potential" $F(\phi_{21}, \phi_{31}) = C$ that determines the dynamics of the coupled neurons, find its critical points associated with FPs—attractors, repellers and saddles of the map, and by scaling f_i predict their bifurcations due to loss of stability, and hence transformations of rhythmic outcomes of the network as a whole.

With such return maps, we can predict and identify the set of robust outcomes in a CPG with mixed, inhibitory and excitatory, slow or/and fast synapses, which are differentiated by phase-locked or periodically varying lags corresponding, respec-
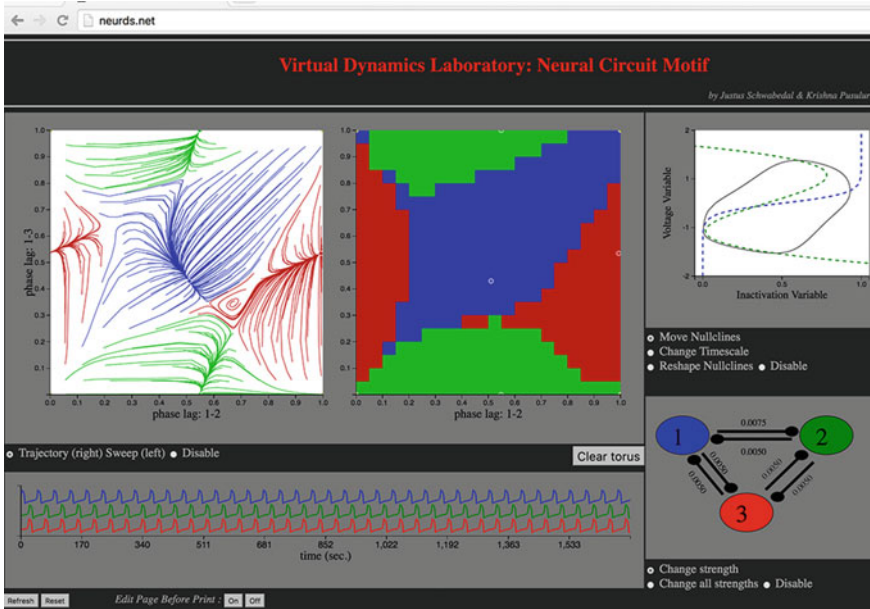
Fig. 5 GPU-based interactive motif-toolbox [56, 57] for computational studies of rhythmogenesis in 3-cell circuits comprised of synaptically coupled FitzhHugh-Nagumo, Hodgkin-Huxley, and 2Θ-neurons, which can generate up to 6 (3 in this figure) robust patterns corresponding to the stable fixed points in the 2D Poincaré return map for the phase lags between constituent cells.

tively, to stable fixed points and invariant circles of the return map. The toolkit lets us predict bifurcations and transformations of rhythmic outcomes before they actually occur in the network. The approach also reveals the capacity of the network and the dependence of its outcomes on coupling strength, wiring circuitry, and synapses, thereby letting one quantitatively and qualitatively identify necessary and sufficient conditions for rhythmic outcomes to occur. Using graphics processor units (GPUs) for parallel simulations of multistable neural networks using multiple initial conditions (as depicted in Fig. 5) can drastically speed up the bifurcation analysis and reduce a simulation time to merely few seconds.

References

1. Hodgkin, A.L., Huxley, A.F.: A quantitative description of membrane current and its application to conduction and excitation in nerve. J. Physiol. **117**(4), 500–544 (1952)
2. Arnold, V.I., Afraimovich, V.S., Ilyashenko, Yu.S., Shilnikov, L.P.: Bifurcation Theory, Vol. V of Dynamical Systems. Encyclopaedia of Mathematical Sciences. Springer (1994)
3. Bertram, R., Butte, M.J., Kiemel, T., Sherman, A.: Topological and phenomenological classification of bursting oscillations. Bull. Math. Biol. **57**(3), 413–439 (1995)
4. Izhikevich, E.M.: Dynamical systems in neuroscience. MIT Press, Cambridge, Mass, The geometry of excitability and bursting (2007)
5. Jones, C.K.R.T., Kopell, N.: Tracking invariant-manifolds with differential forms in singularly perturbed systems. J. Differ. Equ. **108**(1), 64–88 (1994)
6. Rinzel, J.: Bursting oscillations in an excitable membrane model. Lect. Notes Math. **1151**, 304–316 (1985)
7. Rinzel, J., Ermentrout, B.: Analysis of neural excitability and oscillations. In: Koch, C., Segev, I. (eds.) Computational neuroscience, pp. 135–169. MIT Press, Cambridge, Mass (1998)
8. Rinzel, J., Wang, X.J.: Oscillatory and bursting properties of neurons. In Arbib, M. (ed.) The Handbook of Brain Theory and Neural Networks, pp. 686–691. MIT Press (1995)
9. Shilnikov, A.L., Cymbalyuk, G.: Transition between tonic spiking and bursting in a neuron model via the blue-sky catastrophe. Phys. Rev. Lett. **94**(4), 048101 (2005)
10. Shilnikov, A.L., Calabrese, R.L., Cymbalyuk, G.: Mechanism of bistability: tonic spiking and bursting in a neuron model. Phys. Rev. E **71**, 056214 (2005)
11. Channell, P., Cymbalyuk, G., Shilnikov, A.: Origin of bursting through homoclinic spike adding in a neuron model. Phys. Rev. Lett. **98**(13), 134101 (2007a)
12. Channell, P., Cymbalyuk, G., Shilnikov, A.L.: Applications of the poincare mapping technique to analysis of neuronal dynamics. Neurocomputing **70**, 10–12 (2007b)
13. Shilnikov, A., Cymbalyuk, G.: PRL **94**, 048101 (2005)
14. Tikhonov, A.N.: Mat. Sb. **31** 575 (1952); N. Fenichel, J. Diff. Eq. **31**, 53 (1979)
15. Rinzel, J., Ermentrout, B, Koch, C., Segev, I.: Methods in Neuronal Modelling: From Synapses to Networks. MIT Press (1989)
16. Shilnikov, L.P., Shilnikov, A.L., Turaev, D.V., Chua, L.O.: Methods qualitative theory in nonlinear dynamics, Vols. I-II. World Sci. Publ. (1998, 2001); Shilnikov, A.L., Shilnikov, L.P., Turaev, D.V.: Moscow Math J. **5**(1), 205 (2005)
17. Shilnikov, A., Calabrese, R.L., Cymbalyuk, G.: Neurocomputing **65–66**, 869 (2005)
18. Cymbalyuk, G.S., Shilnikov, A.L.: J. Comp. Neuroscience **18**(3), 255 (2004); Regular & Chaotic Dynamics **9**(3), 281 (2004)
19. Wojcik, J., Shilnikov, A.: Voltage interval mappings for activity transitions in neuron models for elliptic bursters. Physica D **240**(14–15), 1164–1180 (2011)
20. Chay, T.R.: Chaos in a three-variable model of an excitable cell. Physica D **16**(2), 233–242 (1985)
21. Griffiths, R.E., Pernarowski, M.C.: Return map characterizations for a model of bursting with two slow variables. SIAM J. Appl. Math. **66**(6), 1917–1948 (2006)
22. Shilnikov, A.L., Rulkov, N.F.: Origin of chaos in a two-dimensional map modelling spiking-bursting neural activity. Int. J. Bifurcation Chaos **13**(11), 3325–3340 (2003)
23. Shilnikov, A.L., Rulkov, N.F.: Subthreshold oscillations in a map-based neuron model. Phys. Lett. A **328**(2–3), 177–184 (2004)
24. Shilnikov, A.L.: On bifurcations of the Lorenz attractor in the Shimizu-Morioka model. Physica D **62**(1–4), 338–346 (1993)
25. Channell, P., Fuwape, I., Neiman, A., Shilnikov, A.L.: Variability of bursting patterns in a neuronal model in the presence of noise. J. Computat. Neurosci. **27**(3), 527–42 (2009)
26. Marder, E., Calabrese, R.L.: Principles of rhythmic motor pattern generation. Physiol Rev. **76**(3), 687–717 (1996)
27. Kristan, W.B., Calabrese, R.L., Friesen, W.O.: Neuronal control of leech behavior. Prog. Neurobiol. **76**, 279 (2005)

28. Calin-Jageman, R.J., Tunstall, M.J., Mensh, B.D., Katz, P.S., Frost, W.N.: Parameter space analysis suggests multi-site plasticity contributes to motor pattern initiation in tritonia. J. Neurophysiol. **98**, 2382 (2007)
29. Newcomb, J.M., Sakurai, A., Lillvis, J.L., Gunaratne, C.A., Katz, P.S.: Homology and homoplasy of swimming behaviors and neural circuits in the nudipleura (mollusca, gastropoda, opistho-branchia). Proc. Natl. Acad. Sci. **109**(1), 10669–76 (2012)
30. Selverston, A. (ed.): Model Neural Networks and Behavior. Springer, Berlin (1985)
31. Bal, T., Nagy, F., Moulins, M.: The pyloric central pattern generator in crustacea: a set of conditional neural oscillators. J. Comparat. Physiol. A **163**(6), 715–727 (1988)
32. Katz, P.S., Hooper, S.L.: Invertebrate central pattern generators. In: North, G., Greenspan, R.R. (eds.) Invertebrate Neurobiology. Cold Spring Harbor Laboratory Press, NY, New York (2007)
33. Marder, E., Calabrese, R.L.: Principles of rhythmic motor pattern generation. Physiol Rev. **76**(3), 687–717 (1996). July
34. Kopell, N., Ermentrout, B.: Chemical and electrical synapses perform complementary roles in the synchronization of interneuronal networks. Proc. Natl. Acad Sci. **101**(43), 15482–15487 (2004)
35. Matsuoka, K.: Mechanisms of frequency and pattern control in the neural rhythms generators. Biol. Cybernetics **1**, 1 (1987)
36. Kopell, N.: Toward a theory of modelling central pattern generators. In: Cohen, A.H., Rossingol, S., Grillner, S. (eds.) Neural Control of Rhythmic Movements in Vertebrates. Wiley, New York (1988)
37. Canavier, C.C., Baxter, D.A., Clark, J.W., Byrne, J.H.: Multiple modes of activity in a model neuron suggest a novel mechanism for the effects of neuromodulators. J Neurophysiol **72**(2), 872–882 (1994). Aug
38. Skinner, F., Kopell, N., Marder, E.: Mechanisms for oscillation and frequency control in networks of mutually inhibitory relaxation oscillators. Comput. Neurosci. **1**, 69 (1994)
39. Dror, R.O., Canavier, C.C., Butera, R.J., Clark, J.W., Byrne, J.H.: A mathematical criterion based on phase response curves for stability in a ring of coupled oscillators. Biol Cybern **80**(1), 11–23 (1999). Jan
40. Prinz, A.A., Billimoria, C.P., Marder, E.: Alternative to hand-tuning conductance-based models: construction and analysis of databases of model neurons. J. Neurophysiol. **90**(6), 3998–4015 (2003). December
41. Belykh, I.V., Shilnikov, A.L.: When weak inhibition synchronizes strongly desynchronizing networks of bursting neurons. Phys. Rev. Lett. **101**(7), 078102 (2008)
42. Shilnikov, A.L., Gordon, R., Belykh, I.: Polyrhythmic synchronization in bursting networking motifs. Chaos **18**(3), 037120 (2008)
43. Sherwood, W.E., Harris-Warrick, R., Guckenheimer, J.M.: Synaptic patterning of left-right alternation in a computational model of the rodent hindlimb central pattern generator. J. Comput Neuroscience **30**(2), 323 (2010)
44. Koch, H., Garcia, A.J., Ramirez, J.-M.: Network reconfiguration and neuronal plasticity in rhythm-generating networks. Integrat. Comparat. Biol. **51**(6), 856–868 (2011)
45. Marder, E.: Neuromodulation of neuronal circuits: back to the future. Neuron **76**, 1 (2012)
46. Calabrese, R.L., Norris, B.J., Wenning, A., Wright, T.M.: Coping with variability in small neuronal networks. Integrat. Comparat. Biol. **51**(6), 845–855 (2011)
47. Kristan, W.B.: Neuronal decision-making circuits. Curr. Biol. **18**(19), R928–R932 (2008). Oct
48. Briggman, K.L., Kristan, W.B.: Multifunctional pattern-generating circuits. Annu. Rev. Neurosci. **31**, 271–294 (2008)
49. Wojcik, J., Clewley, R., Shilnikov, A.L.: Order parameter for bursting polyrhythms in multifunctional central pattern generators. Phys. Rev. E **83**, 056209–6 (2011)
50. Wojcik, J., Clewley, R., Schwabedal, J., Shilnikov, A.L.: Key bifurcations of bursting polyrhythms in 3-cell central pattern generators. PLoS ONE **9**(4) (2014)
51. Jalil, S., Belykh, I., Shilnikov, A.L.: pikes matter in phase-locking of inhibitory bursting networks. Phys. Rev. E. **85**, 36214 (2012)

52. Kopell, N., Somers, D.: Rapid synchronization through fast threshold modulation. Biol. Cybern. **68**, 5 (1993)
53. Marder, E.: Invertebrate neurobiology: polymorphic neural networks. Curr. Biol. **4**(8), 752–754 (1994)
54. Shilnikov, A.L.: Complete dynamical analysis of an interneuron model. J. Nonlinear Dyn. **68**(3), 305–328 (2012)
55. Jalil, S., Allen, D., Youker, J., Shilnikov, A.L.: Toward robust phase-locking in melibe swim central pattern generator models. J. Chaos **23**(4), 046105 (2013)
56. Knapper, D., Schwabedal, J., Shilnikov, A.L.: Qualitative and quantitative stability analysis of penta-rhythmic circuits. Nonlinearity **29**(12), 3647–3676 (2016)
57. Schwabedal, J., Pusuluri, K.: MotifToolBox *https://github.com/jusjusjus/Motiftoolbox* (2016)